# Time-resolved x-ray Raman spectroscopy of photoexcited polydiacetylene oligomer: A simulation study

Satoshi Tanaka[a)]
*Department of Chemistry, University of Rochester, Rochester, New York 14627 and CIAS, Osaka Prefecture University, Sakai 599-8531, Japan*

Sergei Volkov
*Department of Chemistry, University of Rochester, Rochester, New York 14627*

Shaul Mukamel[b)]
*Department of Chemistry, University of Rochester, Rochester, New York 14627 and Department of Physics and Astronomy, University of Rochester, Rochester, New York 14627*

(Received 6 May 2002; accepted 6 November 2002)

Off-resonant x-ray diffraction provides a novel real-space and real-time probe of electronic and vibrational dynamics in optically excited molecules. The entire manifold of valence electronic excitations may be monitored through the dependence of the x-ray Raman peaks on the scattering wave vector $\Delta\mathbf{k}$ and energy $\Delta\omega$. The electronic excitation energies and transition density matrices of a polydiacetylene oligomer, computed using the time-dependent Hartree–Fock collective electronic oscillator algorithm, are used to simulate the Raman signals and illustrate their information content. © *2003 American Institute of Physics.* [DOI: 10.1063/1.1533014]

## I. INTRODUCTION

Recent progress in generating ultrafast x-ray pulses and bringing them down to the attosecond regime has opened up exciting possibilities for novel x-ray spectroscopies.[1–7] Structural changes induced by optical excitation have been investigated by time-resolved x-ray (elastic) diffraction (TRXD)[8–10] and time-resolved x-ray absorption (TRXA) spectroscopies.[11–13] These techniques allow the direct determination of time-resolved structures, in contrast to purely optical techniques which require detailed modeling and computation of potential surfaces to extract such information.

The x-ray diffraction signal may generally be expressed in terms of the *dynamical structural factor* which carries information on the molecular structure as well as on electronic excited states. In that respect, *inelastic* diffraction [time-resolved x-ray Raman, (TRXR)] is similar to time-resolved electron energy loss spectroscopy (TREELS).[14] However, TRXR has several advantages. First, it can investigate the spectrum for higher momentum transfer, making it much more adequate for probing valence excitations with large momentum. Second, electrons are scattered by nuclei and electrons alike, whereas x-ray photons are scattered primarily by electrons, making TRXR much more sensitive to valence electronic excitations. Wilson and coworkers have computed TRXR using a direct extension of the formalism for the stationary x-ray diffraction for the ground state.[15] They discussed the effects of the coherence of the x-ray pulses, the elastic and inelastic scatterings, and quantum interference of the electronic states in TRXR of simple diatomic molecules, such as $I_2$ and $Br_2$, using the independent atomic model (IAM).

We have recently developed a general correlation function formulation of nonlinear x-ray spectroscopies, and used it to describe both TRXR and TRXA in terms of nonlinear response functions.[16] In this article we use this approach to simulate TRXR from a short polydiacetylene chain (Fig. 1) and elucidate its relaxation dynamics in the optically excited state. Very recently, Kobayashi's Group has reported the optical pump–probe absorption of PDA and observed wave packet oscillations corresponding to the C≡C stretching vibration.[17] Optical excitation only detects valence excitations with momentum transfer $\Delta\mathbf{k}=0$; x-ray techniques are not subject to the $\Delta\mathbf{k}=0$ selection rule and can investigate the relaxation dynamics of the entire manifold of valence excited states.

In the most elementary treatment, elastic scattering is calculated by assuming that both electronic and nuclear degrees of freedom are frozen during the process. Cao *et al.* have pointed out that x-ray scattering can directly show the electron dynamics as an interference between the electronic states, provided the duration of the x-ray pulses are so short that their IR bandwidth covers several electronic levels.[15] In this work we show how inelastic TRXR can be effectively used to probe the electronic motions as well as vibrational relaxation dynamics. Previous work which focused on elastic scattering concluded that TRXR under the IAM can only detect the vibrational dynamics.[15] In that case the contribution mostly comes from the time-independent core charge density. In contrast, we show that the electronic dynamics are directly monitored by the Raman peaks even within the IAM, because the wave function, represented by a linear combination of atomic basis states, changes with nuclear configuration.

Our simulations demonstrate how relaxation dynamics of complex molecules may be detected by TRXR. It is a formidable task to obtain the exact many-electron wave

[a)]Electronic mail: stanaka@ms.cias.osakafu-u.ac.jp
[b)]Electronic mail: mukamel@chem.rochester.edu; URL: http://mukamel.chem.rochester.edu

 

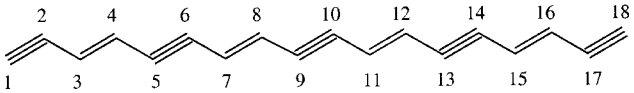


FIG. 1. Molecular structure of the PDA oligomer used in the present simulations.

function of complex molecules. The computation of TRXR has therefore so far been limited to simple molecules, e.g., diatomics.[15] However, we note that in order to obtain the spectrum, we only need to compute the time evolution of the reduced single electron density matrix. This may be easily obtained for large molecules at the time-dependent Hartree–Fock (TDHF) level using the collective electronic oscillator (CEO) technique. The basic formalism is presented in Sec. II. Numerical results are given in Sec. III, followed by a general discussion in Sec. IV.

## II. PROBING ELECTRONICALLY EXCITED MOLECULES WITH X-RAY

In time-resolved x-ray raman scattering (TRXR) experiments the molecule is first brought by an optical pump pulse from the ground state $|g\rangle$ to an excited state $|e\rangle$. After a variable delay time $t_0$, the molecule is probed with an x-ray pulse with a wave vector $\mathbf{k}_i$ and carrier frequency $\omega_i$, and the scattered x-ray radiation ($\mathbf{k}_s$, $\omega_s$) is detected. We denote the momentum transfer $\Delta\mathbf{k}\equiv\mathbf{k}_i-\mathbf{k}_s$, and the energy loss $\Delta\omega\equiv\omega_i-\omega_s$ (the signs of $\Delta\mathbf{k}$ and $\Delta\omega$ are inverted compared to Ref. 16, to warrant the terms ''momentum transfer'' and ''energy loss''). The predominant scattering channel is elastic; however, some x-ray radiation is scattered inelastically, and the energy-loss profile of the TRXR signal reveals the electronic resonances of the molecule. We shall focus on the inelastic (Raman) scattering signal, and demonstrate that it carries detailed information on the electronic state change with vibrational motions. In contrast to optical spectroscopy, the momentum transfer $\Delta\mathbf{k}$ in x-ray scattering can be high; measuring the scattered x-ray versus $\Delta\mathbf{k}$ thus allows the detection of all electronic transitions, not only the optically allowed ($\Delta\mathbf{k}=0$) ones. The time dependent TRXR signal clearly shows the electronic state changes accompanied by the vibrational dynamics induced by the electronic excitation by the optical pump.

The TRXR signal can be formally written as [see Eq. (42) of Ref. 16]:

$$
\begin{aligned}
&W_{\mathrm{TRXR}}(\Delta\omega,\Delta\mathbf{k},t_0)\\
&\quad=-\frac{2}{\omega_i^2}\Re\int d\mathbf{r}\int d\mathbf{r}_3\int_{-\infty}^{\infty}dt\int_0^{\infty}dt_3E_i^*(t)E_i(t-t_3)\\
&\qquad\times\exp[-i\Delta\mathbf{k}\cdot(\mathbf{r}-\mathbf{r}_3)+i\Delta\omega t_3]\\
&\qquad\times\mathrm{Tr}[\hat{\sigma}(\mathbf{r},t)\hat{\sigma}(\mathbf{r}_3,t-t_3)\hat{\rho}^{(2)}(t-t_3)],
\end{aligned}
\tag{1}
$$

where $E_i(t)$ is the electric field envelope of the probing x-ray pulse. Here we have assumed coherent x-ray pulses: To include partial or complete incoherence we need to take the statistical average over the field realizations, $\langle E_i^*(t)E_i(t)\rangle$. For $\Delta\omega=0$ ($\Delta\omega\neq0$) this expression represents elastic (inelastic) x-ray diffraction for the spectral range allowed by the x-ray pulse bandwidth,

$$
\hat{\sigma}(\mathbf{r},t)=e^{i\hat{H}_m(t-t_0)}\hat{\sigma}(\mathbf{r})e^{-i\hat{H}_m(t-t_0)}
\tag{2}
$$

is the electronic charge density operator in the interaction representation,

$$
\hat{\sigma}(\mathbf{r})=e\hat{\psi}^{\dagger}(\mathbf{r})\hat{\psi}(\mathbf{r}),
\tag{3}
$$

and $\hat{H}_m$ is the molecular Hamiltonian. The creation (annihilation) field operators for the electron $\hat{\psi}^{\dagger}(\mathbf{r})$ ($\hat{\psi}(\mathbf{r})$) may be expanded in the atomic basis wave functions:

$$
\begin{aligned}
\hat{\psi}(\mathbf{r})&=\sum_{l,\alpha}\varphi_{l,\alpha}(\mathbf{r}-\mathbf{R}_l)\hat{c}_{l,\alpha},\\
\hat{\psi}^{\dagger}(\mathbf{r})&=\sum_{l,\alpha}\varphi_{l,\alpha}^*(\mathbf{r}-\mathbf{R}_l)\hat{c}_{l,\alpha}^{\dagger},
\end{aligned}
\tag{4}
$$

where $\hat{c}_{l,\alpha}^{\dagger}$ ($\hat{c}_{l,\alpha}$) are creation (annihilation) operators for the electron in the atomic state (spin–orbital) $\alpha$ of the atom $l$, and $\varphi_{l,\alpha}(\mathbf{r}-\mathbf{R}_l)$ is the corresponding atomic basis wave function. We assume that $\varphi_{l,\alpha}(\mathbf{r})$ are orthonormal and do not change with the vibrational motion.

Our calculation starts with the following adiabatic molecular Hamiltonian $\hat{H}_m$:

$$
\hat{H}_m=\sum_{\nu}|\nu\rangle H_m^{(\nu)}(\mathfrak{q})\langle\nu|,
\tag{5}
$$

where $\mathfrak{q}\equiv\{\hat{\mathbf{R}}_l\}$ denotes the complete set of nuclear coordinates and $|\nu\rangle$ is the adiabatic electronic state. The adiabatic eigenstates depend on the nuclear coordinates and $H_m^{(\nu)}(\mathfrak{q})$ is the nuclear Hamiltonian for the $\nu$-th electronic state,

$$
H_m^{(\nu)}(\mathfrak{q})=T(\mathfrak{q})+\Omega_{\nu}(\mathfrak{q}),
\tag{6}
$$

where $T(\mathfrak{q})$ is the nuclear kinetic energy, and $\Omega_{\nu}(\mathfrak{q})$ is the adiabatic potential of state to $|\nu\rangle$.

The time evolution of the total electronic and vibrational density operator $\hat{\rho}^{(2)}(t)$ following the optical pump excitation to second order in the pump field is obtained by solving the quantum Liouville equation and is given in Eq. (33) of Ref. 16.

Expanding the Tr[$\cdots$] in Eq. (1) in the electronic basis we obtain

$$
\begin{aligned}
&W_{\mathrm{TRXR}}(\Delta\omega,\Delta\mathbf{k},t_0)\\
&\quad=-\frac{2}{\omega_i^2}\Re\int d\mathbf{r}\int d\mathbf{r}_3\int_{-\infty}^{\infty}dt\int_0^{\infty}dt_3E_i^*(t)E_i(t-t_3)\\
&\qquad\times\exp[-i\Delta\mathbf{k}\cdot(\mathbf{r}-\mathbf{r}_3)+i\Delta\omega t_3]\\
&\qquad\times\sum_{\nu}\sum_{e,e\beta}\mathrm{Tr}_{\mathfrak{q}}[\langle e|\hat{\sigma}(\mathbf{r},t)|\nu\rangle\langle\nu|\hat{\sigma}(\mathbf{r}_3,t-t_3)|e\beta\rangle\\
&\qquad\times\langle e\beta|\hat{\rho}^{(2)}(t-t_3)|e\rangle].
\end{aligned}
\tag{7}
$$

In our calculations we take the duration of the probing x-ray pulse to be long compared with the electronic time scale $2\pi/|\omega_e-\omega_{\beta}|$, so that we can neglect interferences be-

tween the electronic states of $|e\rangle$ and $|e\beta\rangle$. In this case, using the coherence Green's function defined in the Appendix, the signal is given by

$$W_{\mathrm{TRXR}}(\Delta\omega,\Delta\mathbf{k},t_0) = -\frac{2}{\omega_i^2}\Re\int_{-\infty}^{\infty}dt\int_0^{\infty}dt_3 E_i^*(t)E_i(t-t_3) \times\sum_e\sum_\nu \mu^{e\nu}(\Delta\mathbf{k};\mathrm{q}(t))\mu^{\nu e}(-\Delta\mathbf{k};\mathrm{q}(t-t_3)) \times\exp\left[i\,\Delta\omega\, t_3 - i\int_{t-t_3}^{t}[\Omega_\nu(\mathrm{q}(\tau))-\Omega_e(\mathrm{q}(\tau))]d\tau\right]. \tag{8}$$

Here $\mu^{e\nu}(\Delta\mathbf{k};\mathrm{q}(t))$ is the Fourier transform of the transition matrix element of $\hat{\sigma}(\mathbf{r})$:

$$\mu^{e\nu}(\Delta\mathbf{k};\mathrm{q}) = \int d\mathbf{r}\langle e|\hat{\sigma}(\mathbf{r})|\nu\rangle\exp(-i\,\Delta\mathbf{k}\cdot\mathbf{r}) = \sum_{l,l\beta}\sum_{\alpha,\alpha\beta}\rho^{e\nu}_{l\alpha,l\beta\alpha\beta}\mu_{l\alpha,l\beta\alpha\beta}(\Delta\mathbf{k}), \tag{9}$$

where

$$\mu_{l\alpha,l\beta\alpha\beta}(\Delta\mathbf{k}) = e\int d\mathbf{r}\varphi^*_{l,\alpha}(\mathbf{r}-\mathbf{R}_l)\varphi_{l\beta,\alpha\beta}(\mathbf{r}-\mathbf{R}_{l\beta}) \times\exp(-i\Delta\mathbf{k}\cdot\mathbf{r}). \tag{10}$$

The reduced single-electron transition density matrix between the electronic states $|e\rangle$ and $|\nu\rangle$,

$$\rho^{e\nu}_{l\alpha,l\beta\alpha\beta} = \langle e|c^\dagger_{l,\alpha}c_{l,\beta\alpha\beta}|\nu\rangle, \tag{11}$$

is calculated using the expressions given in Ref. 18. We reiterate that $\rho^{e\nu}$ and $\mu^{e\nu}(\Delta\mathbf{k})$ vary with q through the dependence of the adiabatic eigenstate $|e\rangle$ and $|\nu\rangle$ on nuclear coordinates. We also consider a short Gaussian probe pulse with the width $\Delta T$:

$$E_i(t) = E_i\exp\left[-\frac{(t-t_0)^2}{(\Delta T)^2}\right], \tag{12}$$

where $t_0$ is the time delay between the initial excitation at $t=0$ and the probe. In the impulsive limit where $\Delta T$ is much shorter than all relevant vibrational periods, Eq. (8) may be recast in the form

$$W_{\mathrm{TRXR}}(\Delta\omega,\Delta\mathbf{k},t_0) = -\frac{\pi(\Delta T)^2}{\omega_i^2}|E_i|^2 \times\sum_e\sum_\nu|\mu^{e\nu}(\Delta\mathbf{k};\mathrm{q}(t_0))|^2 \times\exp\{-\tfrac{1}{2}[\Delta\omega-\Omega_\nu(\mathrm{q}(t_0)) +\Omega_e(\mathrm{q}(t_0))]^2(\Delta T)^2\}. \tag{13}$$

We further adopt the independent atom model (IAM),[15,19] which assumes that atomic orbitals are well localized and scatter the x-ray pulse independently and that the atomic scattering does not depend on $\mathbf{R}_l$. $\mu_{l\alpha,l\beta\alpha\beta}(\Delta\mathbf{k})$ is then given by

$$\mu_{l\alpha,l\beta\alpha\beta}(\Delta\mathbf{k}) = \delta_{ll\beta}\exp(-i\Delta\mathbf{k}\cdot\mathbf{R}_l)\,\eta_{l;\alpha\alpha\beta}(\Delta\mathbf{k}), \tag{14}$$

where

$$\eta_{l;\alpha\alpha\beta}(\Delta\mathbf{k}) = e\int_{\mathbf{r}\in l}d\mathbf{r}\,\varphi^*_{l,\alpha}(\mathbf{r})\varphi_{l,\alpha\beta}(\mathbf{r})\exp(-i\Delta\mathbf{k}\cdot\mathbf{r}) \tag{15}$$

is the atomic transition between atomic basis functions $|\alpha\rangle$ and $|\alpha\beta\rangle$ of the $l$-th atom, where the integration of $\mathbf{r}$ is taken within the volume of the atom $l$. Substituting Eqs. (14) and (15) into (9), we have

$$\mu^{e\nu}(\Delta\mathbf{k}) = \sum_l\exp[-i\Delta\mathbf{k}\cdot\mathbf{R}_l]f^{e\nu}_l(\Delta\mathbf{k}), \tag{16}$$

where $f^{e\nu}_l(\Delta\mathbf{k})$ is the atomic scattering factor for the transition $|e\rangle$ to $|\nu\rangle$:

$$f^{e\nu}_l(\Delta\mathbf{k}) = \sum_{\alpha\alpha\beta}\rho^{e\nu}_{l\alpha,l\alpha\beta}\eta_{l;\alpha\alpha\beta} = \sum_{\alpha\alpha\beta}\langle e|c^\dagger_{l\alpha}c_{l\alpha\beta}|\nu\rangle\,\eta_{l;\alpha\alpha\beta}. \tag{17}$$

The outer valence orbital contributes to both elastic and inelastic scattering. We next argue that for valence excitation between $|e\rangle$ and $|\nu\rangle$ in Eq. (17), $|\alpha\rangle$ and $|\alpha\beta\rangle$ must be the same core orbital. This is because in order to have a nonvanishing transition density matrix element, $\langle e|c^\dagger_{l\alpha}c_{l\alpha\beta}|\nu\rangle$, $|e\rangle$ or $|\nu\rangle$ should correspond to different core excited states. The transition energy between $|e\rangle$ and $|\nu\rangle$ will be extremely high, corresponding to the core excitation energy, which is beyond the scope of the present study. Therefore, if the atomic orbital $|\alpha\rangle$ or $|\alpha\beta\rangle$ is a core state, then $|\alpha\rangle=|\alpha\beta\rangle$ and the core level only contributes to elastic scattering,

$$f^{e\nu}_{l;\mathrm{core}}(\Delta\mathbf{k}) = \delta_{e\nu}\int_{\mathbf{r}\in l}\sum_{\alpha\in\mathrm{core}}|\varphi_{l\alpha}(\mathbf{r})|^2\exp[-i\Delta\mathbf{k}\cdot\mathbf{r}]. \tag{18}$$

The core orbitals become essential for energy loss corresponding to core excitation energy.

When the x-ray wavelength is much longer than the atomic size, we can expand the $\exp(-i\Delta\mathbf{k}\cdot\mathbf{r})$ factor, and have

$$\eta_{l;\alpha\alpha\beta}(\Delta\mathbf{k}) = [e\,\delta_{\alpha\alpha\beta} - i\Delta\mathbf{k}\cdot\mathbf{d}_{l;\alpha,\alpha\beta}], \tag{19}$$

where $\mathbf{d}_{l;\alpha,\alpha\beta}$ is the transition dipole moment between atomic orbitals $|\alpha\rangle$ and $|\alpha\beta\rangle$ of the $l$-th atom:

$$\mathbf{d}_{l;\alpha,\alpha\beta} = e\int d\mathbf{r}\varphi^*_{l,\alpha}(\mathbf{r})\mathbf{r}\varphi_{l,\alpha\beta}(\mathbf{r}). \tag{20}$$

From Eqs. (16) and (19), we obtain

$$\mu^{e\nu}(\Delta\mathbf{k}) = \sum_l\exp[-i\Delta\mathbf{k}\cdot\mathbf{R}_l](\rho^{e\nu}_l - i\Delta\mathbf{k}\cdot\boldsymbol{\xi}^{e\nu}_l), \tag{21}$$

where

$$\rho^{e\nu}_l \equiv e\sum_\alpha\langle e|c^\dagger_{l\alpha}c_{l\alpha}|\nu\rangle \tag{22}$$

is the net charge induced on the $l$-th atomic orbital by the external field, and

$$\boldsymbol{\xi}_l^{e\nu}=\sum_{\alpha\alpha\beta}\langle\nu|c_{l\alpha}^{\dagger}c_{l\alpha\beta}|\nu\rangle\mathbf{d}_{l;\alpha,\alpha\beta} \tag{23}$$

is the atomic transition dipole probability on the $l$-th atom.

For molecules with translational symmetry (e.g., conjugated polyenes), the atomic position may be represented by the relative displacement from the center of the unit cell $\mathbf{R}_m$,

$$\mathbf{R}_l=\mathbf{R}_m+\mathbf{R}_{l(m)}, \tag{24}$$

where $\mathbf{R}_{l(m)}$ is the atomic position within the $m$-th unit cell. From Eqs. (16) and (24), we then have

$$\mu^{e\nu}(\Delta\mathbf{k})=F^{e\nu}(\Delta\mathbf{k})\sum_m \exp[-i\Delta\mathbf{k}\cdot\mathbf{R}_m], \tag{25}$$

where the structure factor,

$$F^{e\nu}(\Delta\mathbf{k})=\sum_{l\in m}\exp[-i\Delta\mathbf{k}\cdot\mathbf{R}_{l(m)}]f_{l(m)}^{e\nu}(\Delta\mathbf{k}), \tag{26}$$

and the factor $\Sigma_m \exp[-i\Delta\mathbf{k}\cdot\mathbf{R}_m]$ gives the Bragg diffraction condition.

In the next section we use these expressions to calculate TRXR spectra.

## III. NUMERICAL RESULTS

We have simulated TRXR of the polydiacetylene (PDA) oligomer (Fig. 1), in the impulsive x-ray probe pulse limit using the IAM. The calculations use Eqs. (13), (16), and (17). We assume that the pump bandwidth only covers the first peak of the lowest energy absorption peak attributed to the excitation to the first excited $^1B_u$ state[20] and hereafter we denote $|e\rangle$ as the $^1B_u$ excited state. We therefore only retain the $^1B_u$ state in the sum over $|e\rangle$ in (13). This optical pulse excitation induces the vibrational motion investigated by Tommasini *et al.*[20]

We used the CEO code which is particularly suitable for simulating electronic excitations of closed-shell molecules.[21,22] The CEO modes and the corresponding frequencies $\Omega_\nu$ were calculated following the procedures described earlier,[22] using the INDO/S semiempirical Hamiltonian as parametrized by Zerner and co-workers[24] in the ZINDO code. The Hartree–Fock self-consistent field procedure is first used to compute the reduced ground-state electronic density matrix $\rho^{gg}$. We then calculated the fifty lowest-frequency CEO modes, using the oblique Lanczos algorithm for finding the eigenvectors of the sparse Liouville-space matrix. The trajectory of the nuclear coordinates $\mathfrak{q}$ was obtained by solving the classical equations of motion in the electronic excited state $|\nu\rangle$:[20]

$$m_\alpha\ddot{\mathfrak{q}}_\alpha=-\frac{d}{d\mathfrak{q}_\alpha}[E_0(\mathfrak{q})+\Omega_\nu(\mathfrak{q})], \tag{27}$$

where $m_\alpha$ is the effective mass of $\mathfrak{q}_\alpha$ and $E_0(\mathfrak{q})$ is the ground-state energy. Equation (27) was solved numerically using the MDCEOV molecular-dynamics code[20] which implements the Verlet algorithm.

We have used the 1-ps molecular-dynamics trajectory $\mathfrak{q}(t)$ in the lowest electronic excited state $|e\rangle$ computed in Ref. 20 with a 0.5-fs time step to calculate the $W_{\mathrm{TRXR}}$ [Eq. (13)] for various time delays $t_0$. The probe duration $\Delta T=3$ fs, which is shorter than all vibrational periods of the molecule, is short enough to justify Eq. (13), yet sufficiently long to resolve the various resonances.

In Fig. 2 we present the TRXR versus the energy loss $\Delta\omega$ for several values of $\Delta\mathbf{k}$ parallel to the molecular axis: (a) $\Delta\mathbf{k}=0.001$ Å$^{-1}$, (b) 0.2 Å$^{-1}$, (c) 0.4 Å$^{-1}$, and (d) 0.6 Å$^{-1}$. Since x-ray scattering by core orbitals contributes to time-independent elastic scattering, we only show the Raman peaks which correspond to the valence excitations and deleted the intense elastic $\Delta\omega=0$ peak. For these relatively small values of $\Delta\mathbf{k}$ only the charge density contributes to the transition matrix element of Eq. (21):

$$\mu^{e\nu}(\Delta\mathbf{k})=\sum_l \exp[-i\,\Delta\mathbf{k}\cdot\mathbf{R}_l]\rho_l^{e\nu}. \tag{28}$$

Fourier transform of the wave vector dependence of TRXR thus yields the induced charge density for the $|e\rangle$ to $|\nu\rangle$ transition state. Using Eq. (9) we have

$$\mu^{e\nu}(\Delta\mathbf{k}=0)=\langle e|\int d\mathbf{r}\,\hat{\sigma}(\mathbf{r})|\nu\rangle=\langle e|\hat{N}|\nu\rangle, \tag{29}$$

where $\hat{N}$ is the total electron number operator. Since $[\hat{N},\hat{H}_m]=0$, $\mu^{e\nu}=N\delta_{e\nu}$, where $N$ is the total number of electrons. This means that only the elastic peak survives when $\Delta\mathbf{k}=0$.

For $\Delta\mathbf{k}=0.001$ Å$^{-1}$ (a), the $\Delta\omega=-2$ eV peak whose central frequency oscillates with a 10-fs period is attributed to the $|e\rangle$ to $|g\rangle$ transition. Since $\Delta\mathbf{k}$ is small, only final states with a long wavelength transition charge density can be detected. The induced charge density between $|e\rangle$ and $|g\rangle$ has a very long wavelength, as shown below, which can be also detected by a nonlinear optical, such as pump–probe, spectroscopy. The 10-fs period corresponds to C≡C stretching vibrations (see Fig. 9 in Ref. 20). On the other hand, the $\Delta\omega=1.8$ eV peak only shows a weak variation with time, indicating that the adiabatic potential surface for this state is almost parallel to that of $|e\rangle$.

In Fig. 3 we show the TRXR intensities $|\mu^{e\nu}(\Delta\mathbf{k};t_0=0)|^2$ for the same $\Delta\mathbf{k}$ values of Fig. 2, on an expanded scale. The number in the bracket denotes the state number $|\nu\rangle$ where $\nu=1$ is the lowest excited state, etc. The elastic scattering intensities without the core orbital contribution are shown by thick arrows at $\Delta\omega=0$ eV and their total intensities are indicated on top. Since the valence excited states with higher momentum have larger energies, the spectra shift towards higher $\Delta\omega$ as $\Delta\mathbf{k}$ is increased. The overall $\Delta\mathbf{k}$ dependence of TRXR for $t_0=0$ is shown in Fig. 4, where the open circle at $\Delta\omega=0$ corresponds to the elastic peak. The scattering for each value of $\Delta\omega$ is peaked in a narrow range of $\Delta\mathbf{k}$. This reflects an approximate translational symmetry; for infinite chains $\mathbf{k}$ is a good quantum number and each value of $\Delta\omega$ should correspond to a specific value of $\Delta\mathbf{k}$.

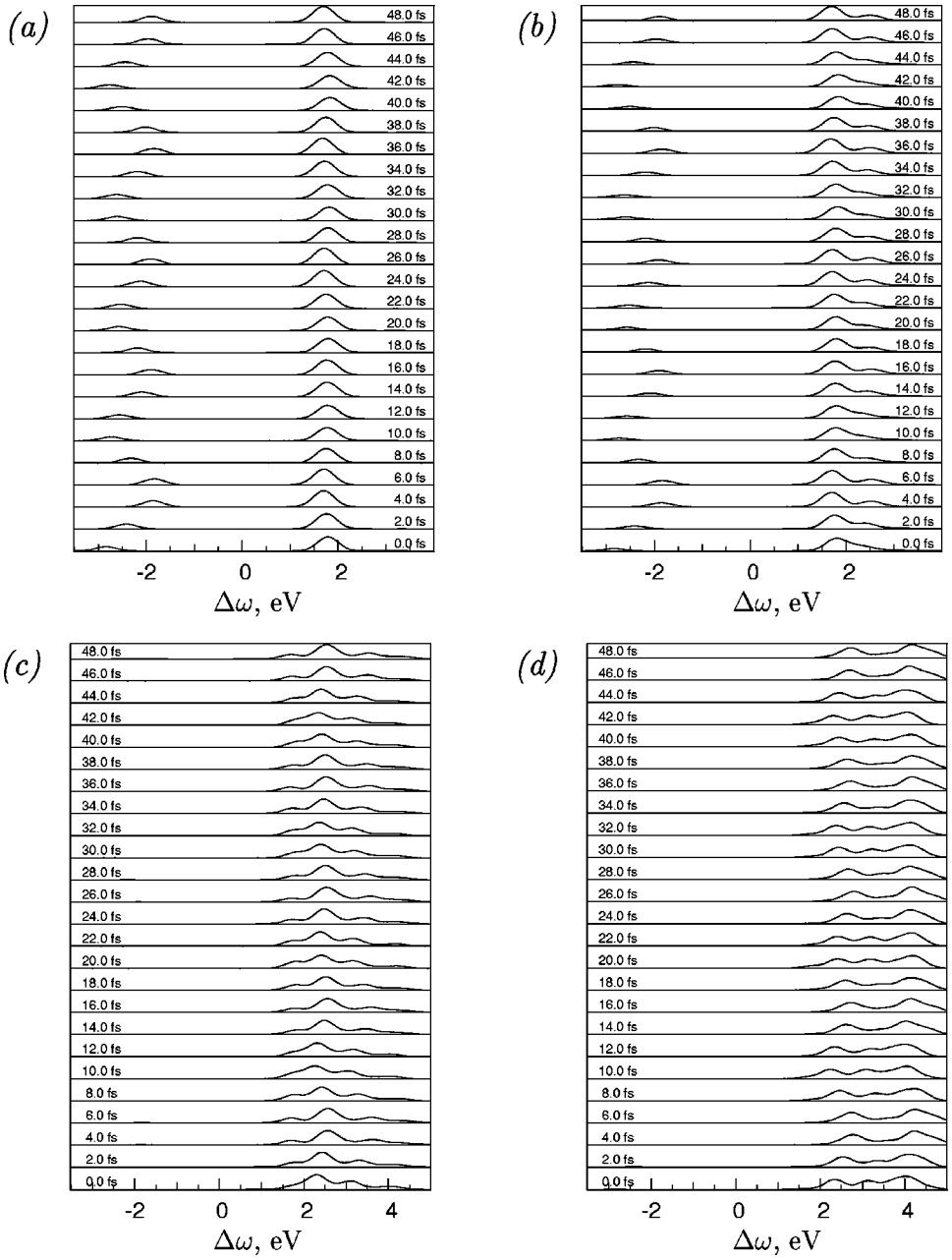


FIG. 2. Time-resolved x-ray Raman scattering signal for the polydiacetylene oligomer plotted vs the energy loss of the scattered x-rays for different delay times $t_0$ between the optical pump and x-ray probe. The x-ray probe pulse halfwidth is $\Delta T=3$ fs, the momentum transfer is 0.001 $\text{Å}^{-1}$ (a), 0.2 $\text{Å}^{-1}$ (b), 0.4 $\text{Å}^{-1}$ (c), 0.6 $\text{Å}^{-1}$ (d) and directed along the molecule. The TRXR signal is plotted on an arbitrary scale, different for each panel.

It is interesting to examine the ratio of the elastic and the inelastic scattering peak intensities. From Eq. (9) the intensity of the elastic scattering peak is represented by

$$|\mu^{ee}(\Delta\mathbf{k})|^2=\int d\mathbf{r}_1\int d\mathbf{r}_2\, e^{-i\Delta\mathbf{k}(\mathbf{r}_1-\mathbf{r}_2)} \times\langle e|\hat{\sigma}(\mathbf{r}_1)|e\rangle\langle e|\hat{\sigma}(\mathbf{r}_2)|e\rangle. \tag{30}$$

On the other hand, the total sum of the inelastic scattering peaks is

$$\sum_\nu |\mu^{e\nu}(\Delta\mathbf{k})|^2=\int d\mathbf{r}_1\int d\mathbf{r}_2\, e^{-i\Delta\mathbf{k}(\mathbf{r}_1-\mathbf{r}_2)} \times\langle e|\hat{\sigma}_2(\mathbf{r}_1,\mathbf{r}_2)|e\rangle, \tag{31}$$

where $\hat{\sigma}_2(\mathbf{r}_1,\mathbf{r}_2)$ is the two-particle density operator defined by

$$\hat{\sigma}_2(\mathbf{r}_1,\mathbf{r}_2)\equiv\hat{\psi}^\dagger(\mathbf{r}_1)\hat{\psi}^\dagger(\mathbf{r}_2)\hat{\psi}(\mathbf{r}_2)\hat{\psi}(\mathbf{r}_1); \tag{32}$$

the sum of all inelastic scattering peaks given by subtracting Eq. (30) from (31) represents the spatial correlation of the electrons in the state $|e\rangle$.

The $\Delta\mathbf{k}$ dependence of TRXR is related to the transition density matrices $\rho^{e\nu}_{l\alpha,l\beta\alpha\beta}$ for the transitions to the final states $|\nu\rangle$ which dominate the TRXR spectrum in Fig. 3: These are shown in the site representation in Fig. 5. The transition to (a) the ground state, (b) $\nu=14$, (c) $\nu=17$, (d) $\nu=27$, (e) $\nu=36$, and (f) $\nu=40$. The corresponding frequencies are indicated in each panel. The site labelling used in this figure is given in Fig. 1. The $x$ and $y$ axes represent the electron and hole location, respectively, at atoms $l$ and $l\beta$ in the $|e\rangle$ to $|\nu\rangle$ transition. The color code shows an increase of the transition-induced change in the coherence between the cor-

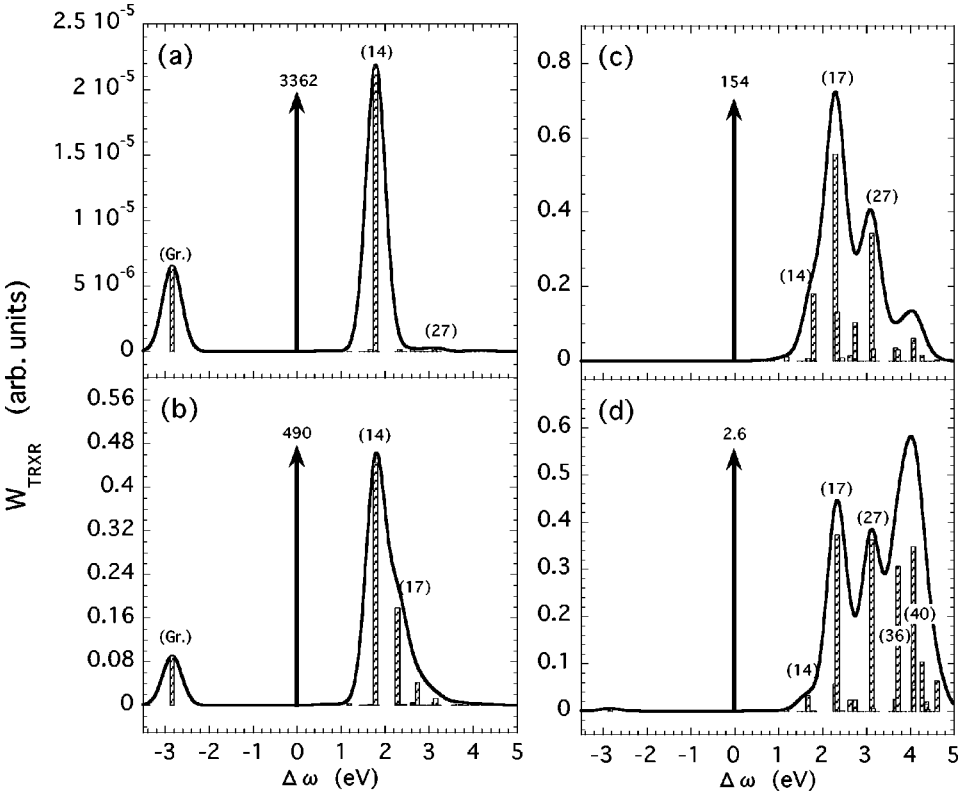


FIG. 3. The TRXR intensities $|\mu^{e\nu}(\Delta\mathbf{k};t_0=0)|^2$ for various values of $\Delta\mathbf{k}$'s corresponding to Fig. 2.

responding atoms $l$ and $l\beta$ from blue to red; $\rho^{e\nu}_{l\alpha,l\beta\alpha\beta}$ differs by a factor of 2 for consecutive rainbow colors. The upper left panel in Fig. 5 corresponds to the transition from the first electronic excited state $|e\rangle$ to the ground state $|g\rangle$, $\rho^{eg}$, the next panel shows the density matrix in the state $|e\rangle$, $\rho^{ee}$ which is responsible for elastic scattering, and the remaining panels show the transitions from $|e\rangle$ to higher-lying electronic excited states $|\nu\rangle$. The diagonal and off-diagonal elements of these matrices represent the induced charge density and the dynamical bond-order corresponding to the joint amplitude of finding an electron on $l$ and a hole on $l\beta$ site associated with the transition from $|e\rangle$ to $|\nu\rangle$, respectively. These types of density matrix plots are described in detail in Ref. 22. The transition density matrices for the lowest 50 excited states are given in EPAPS.[23]

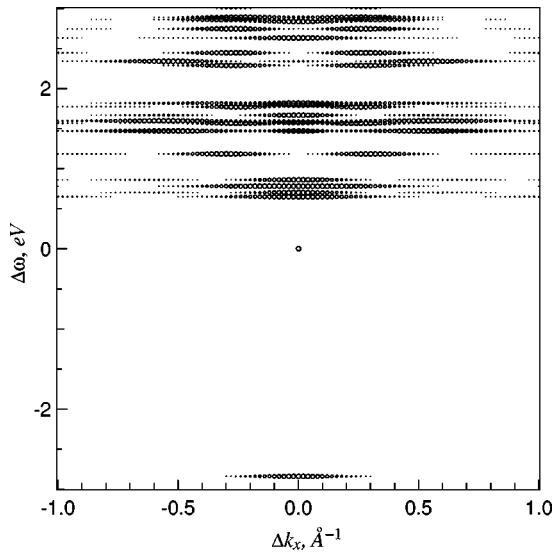


FIG. 4. The $\Delta k$ dependence of $W_{\mathrm{TRXR}}(\Delta\mathbf{k},\Delta\omega,t_0=0)$, with $\Delta\mathbf{k}$ directed along the molecular axis ($x$ axis). Normalization for each frequency (i.e., for each horizontal line) is performed for clarity. The radius of each circle is proportional to the relative normalized intensity at a given point in the $(\Delta\omega,\Delta k_x)$ plane.

As can be seen from Eq. (28), the TRXR signal depends only on the diagonal elements of the density matrix (induced charges). In Fig. 6 we display the diagonal density matrix element of the transition density matrix $\rho^{e\nu}_l$ [Eq. (22)] for the same transitions as in Fig. 5. The solid lines are to guide the eye.

PDA possesses inversion symmetry with respect to the center, and the induced charge density wave is characterized by the same symmetry: The charge density waves in panels (a), (b), and (d) are asymmetric, whereas (c), (e), and (f) are symmetric. We also plot a least square linear fit (dashed lines): The finite slope of this line indicates that the long range charge redistribution happens between both blocks for the $|e\rangle$ to $|\nu\rangle$ with the electronic transition. This means that a long range dipole moment is induced by this transition which can only be detected when $\Delta\mathbf{k}$ is very small, i.e., in the long wavelength limit. From Fig. 6 we can see the large induced charge density for the transition of $|e\rangle\rightarrow|g\rangle$ (a), $|e\rangle\rightarrow|\nu=14\rangle$ (b), and the slight induced charge density in $|e\rangle\rightarrow|\nu=27\rangle$ (d), which is in good agreement with the peak intensity in Fig. 3(a). On the other hand, in (c), (e), and (f), which lack a long range charge density, the TRXR has a significant intensity only when $\Delta\mathbf{k}$ becomes large enough to observe the changes within each box.

Similarly we can observe the strong $\Delta\mathbf{k}$ dependence of the stationary x-ray inelastic scattering from the ground state.

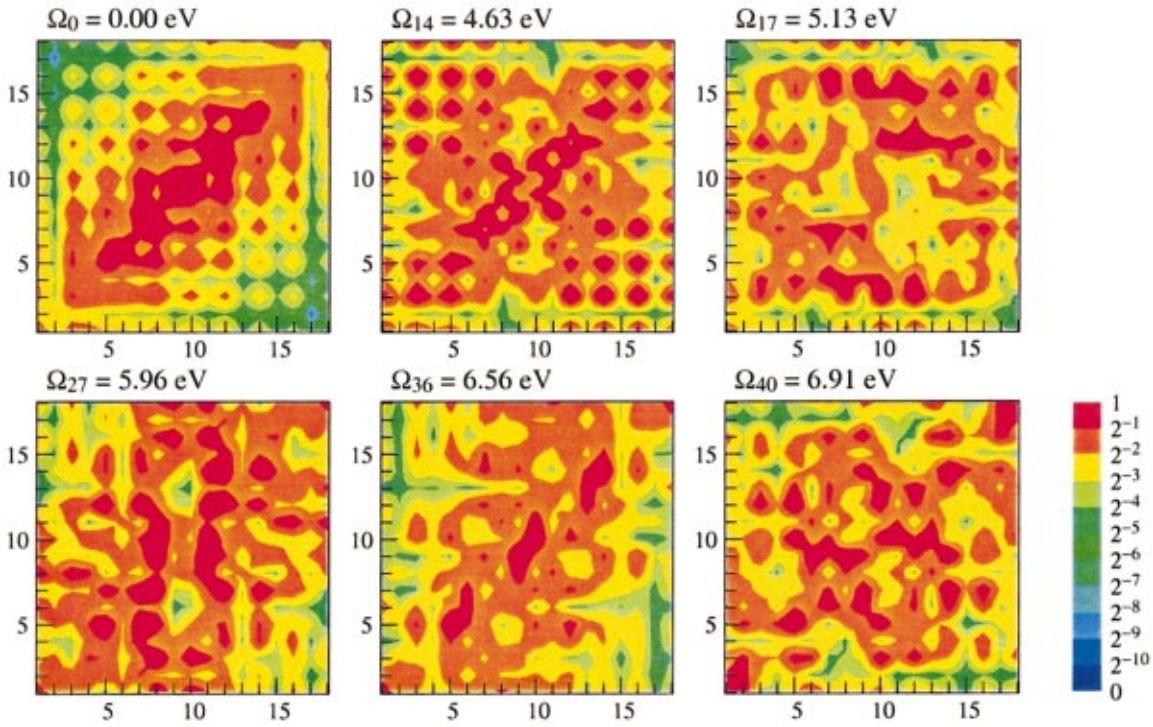


FIG. 5. (Color) Transition density matrices $\rho^{e\nu}_{l\alpha,l\beta\alpha\beta}$ for the transitions to the final states $|\nu\rangle$ which dominate the TRXR spectrum in Fig. 3. The transition to $\nu=$ (a) Ground state, (b) 14-, (c) 17-, (d) 27-, (e) 36-, (f) 40th excited states. $\rho^{e\nu}_{l\alpha,l\beta\alpha\beta}$ are drawn for $t_0=0$ on a logarithmic scale. The $x$ and $y$ axes are labeled by the carbon atoms $l$ and $l\beta$. For each $l$ and $l\beta$, mean-square averaging is performed over all pairs atomic orbitals $\alpha$ and $\alpha\beta$ (see Ref. 27). The carbon atoms are numbered consecutively from one end of the molecule to the other.

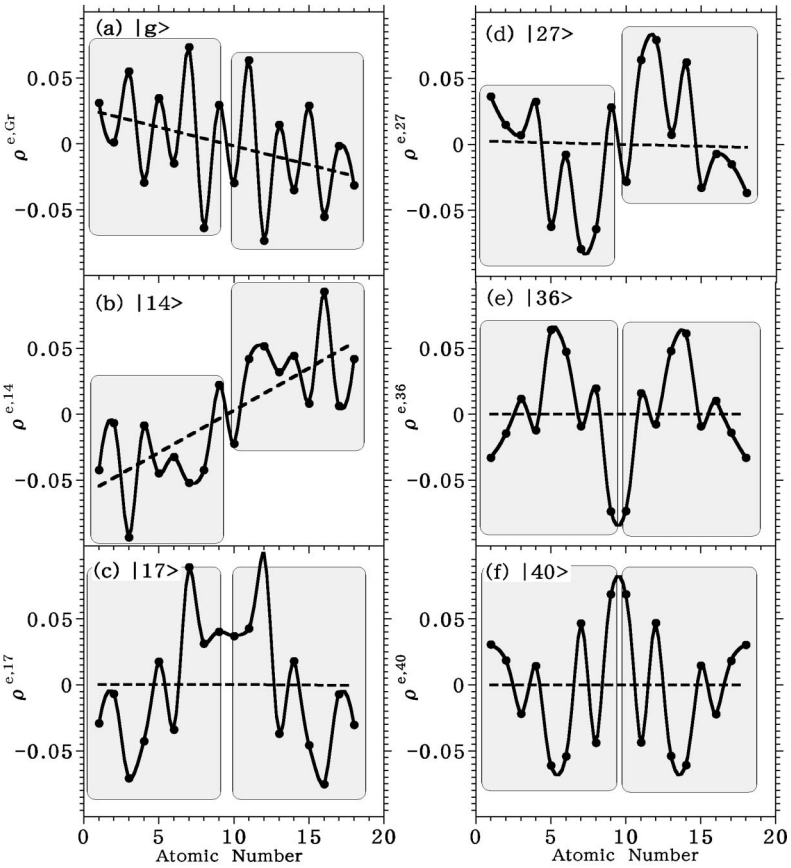


FIG. 6. The diagonal matrix elements of the transition density matrix $\rho^{e\nu}_{l}$ in Fig. 5. The solid lines are to guide the eyes and the dashed lines are the least square linear fit for them.

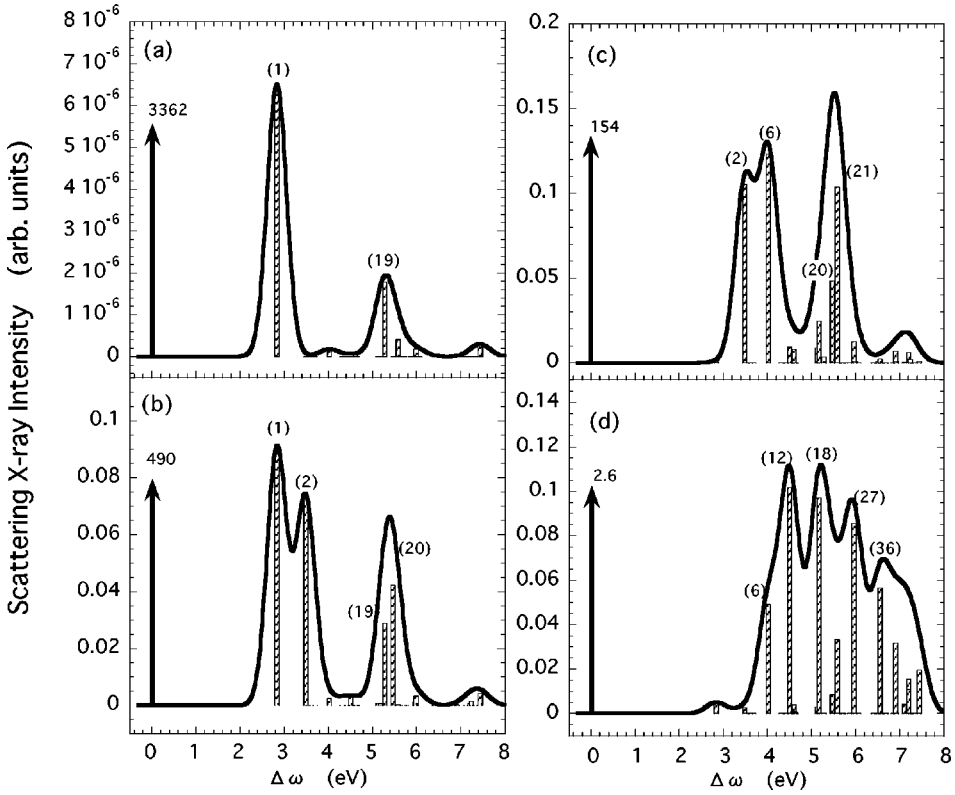


FIG. 7. The stationary x-ray inelastic scattering spectra for various values of $\Delta\mathbf{k}$.

The x-ray inelastic scattering peaks for the same values of momentum transfer of Fig. 3 are shown in Fig. 7, where the excited state number is given in the bracket. When $\Delta\mathbf{k}=0.001$ Å$^{-1}$ (a), we see two prominent inelastic peaks at $\Delta\omega=2.84$ eV and 5.28 eV corresponding to $\nu=1$ and the $\nu=19$, respectively. The $\Delta\omega=2.84$ eV peak is due to the excitation from the ground state to $|e\rangle$ which is the counterpart of the $\Delta\omega=-2.84$ eV peak in Fig. 3 due to the deexcitation from $|e\rangle$ back to the ground state. The absence of the strong peak corresponding to the $\nu=14$ in Fig. 3(a) reflects the different selection rules between the transitions from the ground state (Fig. 7) and from the first excited state (Fig. 3). As $\Delta\mathbf{k}$ is increased, additional inelastic peaks appear which are shifted towards higher energy, just as in Fig. 3.

The transition density matrices from the ground state to state $\nu$, $\rho^{g\nu}_{l\alpha,l\beta\alpha\beta}$, are shown in Fig. 8 where those corresponding to the transitions dominate the x-ray inelastic scattering peaks in Fig. 7 are shown in Fig. 8: Each panel corresponds to one of the peaks of Fig. 7. We use the same color code as in Fig. 5. The transition density matrices for the lowest 50 excited states are given in EPAPS.[23] In Fig. 9 we display the diagonal matrix elements of the density matrix $\rho^{g\nu}_{l}$, defined by replacing $\langle e|$ with $\langle g|$ in Eq. (23). As noted in Fig. 6, for $\Delta\mathbf{k}=0.001$ Å$^{-1}$, only when the long range charge density is induced [Figs. 9(a) and 9(f)], we see inelastic x-ray scattering peaks in Fig. 7(a).

As may be seen in Fig. 3, the temporal variation in relative intensities of the Raman peaks becomes more pronounced for larger $\Delta\mathbf{k}$. To illustrate this, we show in Fig. 10 a bar diagram depicting the time dependent TRXR for $\Delta\mathbf{k}=0.6$ Å$^{-1}$, where the elastic peaks are omitted for clarity. The relative intensities change periodically following the periodic stretching C≡C vibration; the spectra are very similar for (a) $t_0=0$ fs and (e) $t_0=32$ fs, and for (c) $t_0=16$ fs and (g) $t_0=48$ fs. The former pair corresponds to the minimum amplitude of the C≡C stretches and the latter to the maximum (see Fig. 9 in Ref. 20).

The time dependent induced charge densities corresponding to the major peaks in Fig. 10 are shown in Fig. 11 for $t_0=0$ fs [(a)–(d)], 8 fs [(e)–(h)], and 16 fs [(i)–(j)]. Since $\Delta\mathbf{k}$ is large (0.6 Å$^{-1}$), the TRXR can detect the induced charge density even though it does not show long range induced polarization with the transition. In fact, the induced charge density changes with time even though there is no global (long range) induced polarization. Since this local induced charge density is strongly affected by the molecular structure change with the C≡C stretching vibration, the relative intensities of the inelastic scattering peaks are affected more strongly compared to small $\Delta\mathbf{k}$. The TRXR signal thus reflects the close relationship between dynamical change of the excited states and the molecular structure.

## IV. CONCLUDING REMARKS

In this paper we have simulated TRXR of PDA by combining the formalism developed in Ref. 16 with the CEO algorithm for computing the electronic excitations, based on the reduced single electron density matrix. The molecular dynamics trajectory following an impulsive excitation to the first excited $^1B_u$ state was calculated in Ref. 20. The present simulations show that TRXR is a powerful technique for investigating the joint electronic and vibrational motion induced by the optical excitation as well as the molecular structural changes. They clearly illustrate how the time de-

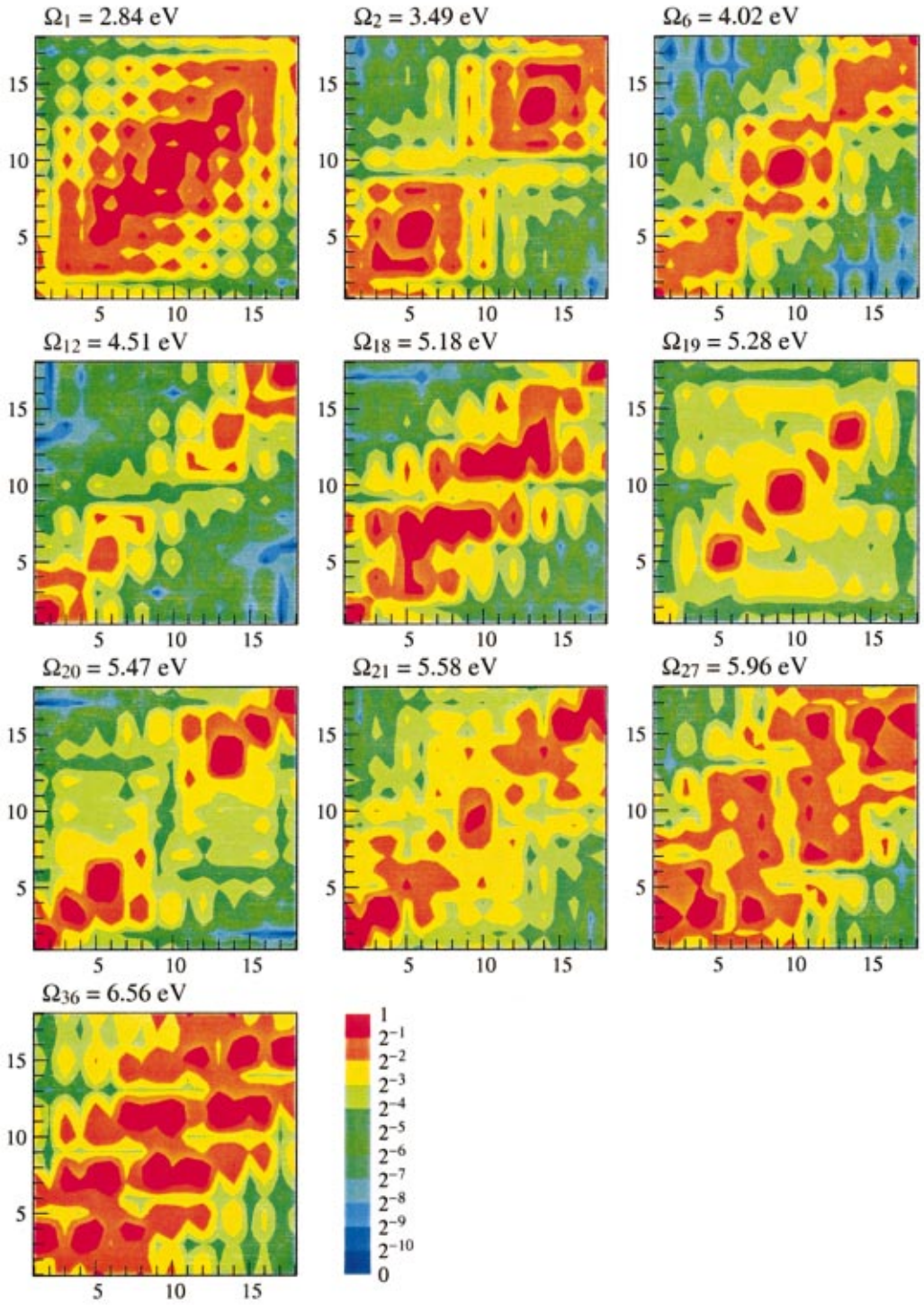


FIG. 8. (Color) Transition density matrices $\rho^{g\nu}_{l\alpha,l\beta\alpha\beta}$ from the ground state to the excited state of the polydiacetylene oligomer which dominate the spectrum in Fig. 7: The transition to $\nu=$ (a) 1-, (b) 2-, (c) 6-, (d) 12-, (e) 18-, (f) 19-, (g) 20-, (h) 21-, (i) 27-, and (j) 36th excited states. $\rho^{g\nu}_{l\alpha,l\beta\alpha\beta}$ are drawn in the same way as in Fig. 5.

pendent inelastic TRXR peaks reflect the electronic relaxation dynamics along with the photoinduced vibrational motion. TRXR has a distinct $\Delta\mathbf{k}$ dependence, which allows us to extract the time evolution of the induced charge density. Specifically, as $\Delta\mathbf{k}$ is increased, the TRXR signal can probe the short wavelength change of the charge density, which is sensitive to the stretching motion along the molecular axis.

Wilson *et al.* had argued that within the IAM it is impossible to observe electronic state dynamics, and only real time vibrational motion may be observed.[15] But as shown here, we can detect the electronic state change with time through the inelastic scattering peaks. This is because the coefficients of the adiabatic eigenstates change with the vibrational motion, and the inelastic scattering peak intensities contain direct signatures of these changes.

We have assumed that the atomic basis functions are

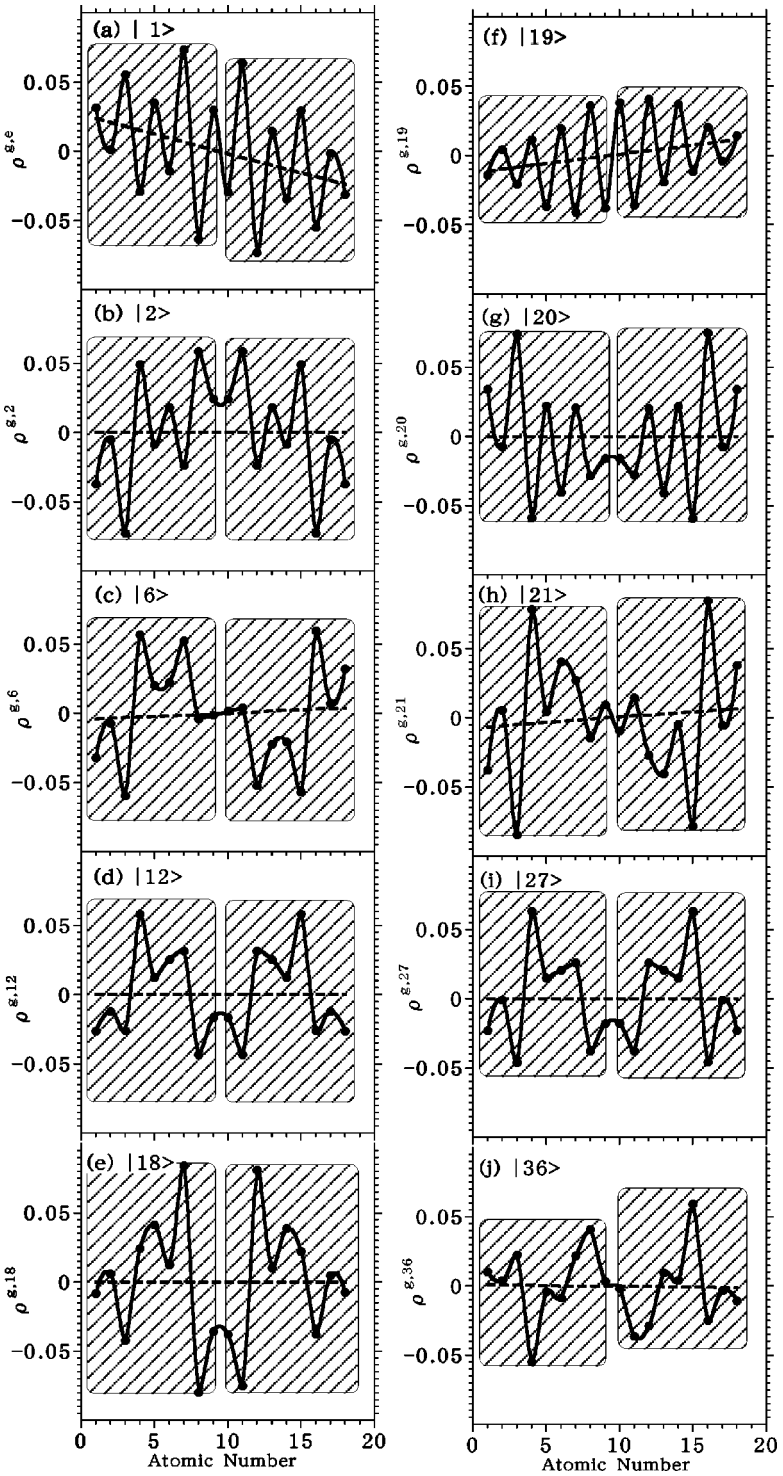


FIG. 9. The diagonal matrix elements of the transition density matrix $\rho_I^{g\nu}$ in Fig. 8.

localized at the various atomic sites and neglected the interatomic transition matrix element of the charge density in Eq. (15). Even though the *intra-atomic* transitions should dominate the transition matrix elements, *interatomic* transitions may contribute to the spectrum as well because the atomic functions may overlap for the outer valence states. In that case, TRXR can probe not only the induced charge density represented by the diagonal density matrix element but also the temporal change of the *bond order* represented by the off-diagonal density matrix elements. We can thus detect how the coherence of the electronic states is changed along with the vibrational motion. This should provide a novel and unique insight into electronic structure which is not possible by any other technique.

According to recent pump–probe experiments in PDA[17] and theoretical analysis,[20] the bending motion between the double bond and the triple bond is induced by the optical excitation to the $^1B_u$ state. Consequently, we may probe not only the induced charge density along the bond axis, but the perpendicular direction as well. We can thus obtain the three dimensional image for the change of the induced charge den-

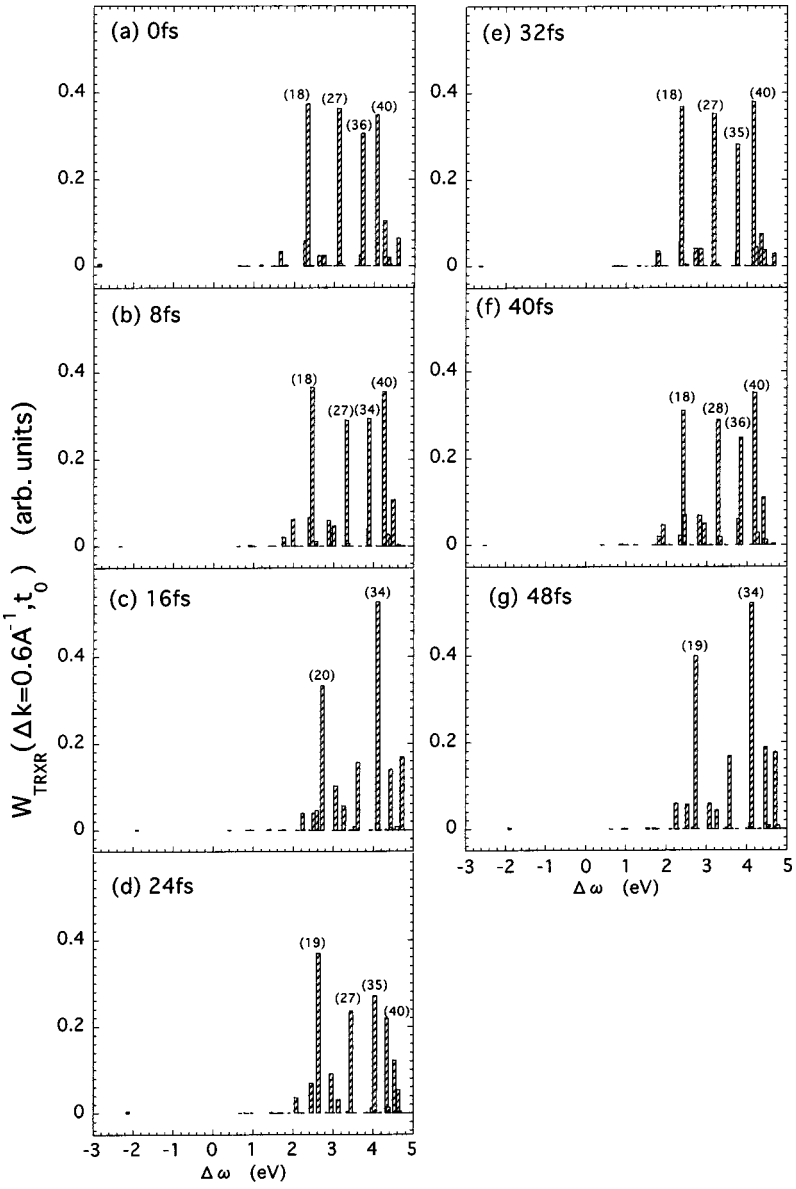


FIG. 10. The temporal change of TRXR for $\Delta\mathbf{k}=0.6$ Å$^{-1}$: $t_0=0$ fs (a), 8 fs (b), 16 fs (c), 24 fs (d), 32 fs (e), 40 fs (f), and 48 fs (g).

sity and follow the real-time motion for the electronic wavepacket after the optical excitation.

Finally, it will be interesting to compare the TRXR with time-resolved EELS.[14] The expression used here [Eqs. (13), (16), and (17)] can also be applied to the analysis for EELS by simply replacing $f_l^{e\nu}(\Delta\mathbf{k})$ in Eq. (16) with

$$g_l^{e\nu}(\Delta\mathbf{k})=\frac{1}{\Delta\mathbf{k}^2}[Z_l-f_l^{e\nu}(\Delta\mathbf{k})], \tag{33}$$

where $Z_l$ is an atomic number of the atom $l$. The reason is that the incoming electron is scattered by the electrostatic potential originating from both nuclei and electrons, whereas x-rays interact primarily with the electrons. It should be noted that this expression can be used within the first Born approximation only, i.e., the incoming electron kinetic energy is very high and its coupling with the molecule is taken into account to first order. In this case, the scattered electron is detected by transmission through the sample (forward scattering configuration) and the sample should be prepared in thin film. However, since the electron energy is very high (typically several hundred keV) and the molecular electron wavelength is much shorter ($\simeq 0.02$ Å ) than the interatomic distance, the detectable momentum transfer is restricted to a very small $\Delta\mathbf{k}$ region. Probing the high $\Delta\mathbf{k}$ region requires reducing the incoming electron energy, but in this case the interaction of the electron and the molecule may no longer be described by the first Born approximation; we have to take into account multiple scattering effects which complicates the analysis.[25] In contrast, x-ray diffraction can easily detect large momentum transfers.

In the present calculations, we did not incorporate nonadiabatic transitions between electronic states because the $^1B_u$ state is energetically isolated from the other electronic states. However, when the molecule is strongly deformed, such as in the course of photoisomerization, nonadiabatic transitions may become important, resulting in interferences between the $|e\rangle$ and $|e\delta\rangle$ states in Eq. (7). This will be an interesting topic for a future study.

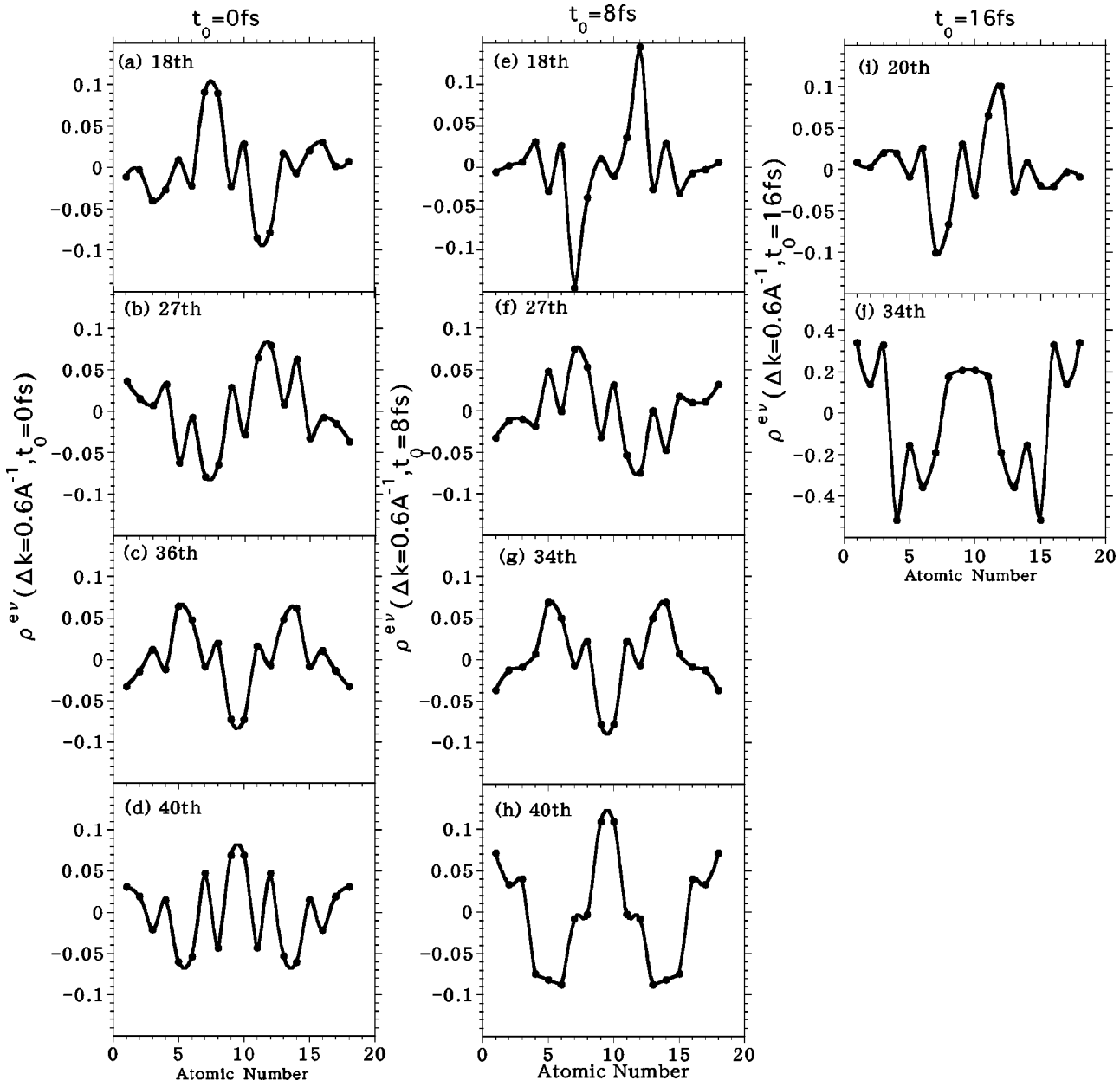


FIG. 11. The temporal change of the induced charge density of $\Delta\mathbf{k}=0.6$ Å$^{-1}$ for $t_0=0$ fs [(a)–(d)], 8 fs [(e)–(h)], and 16 fs [(i)–(j)]. The charge densities corresponding to the numbered major peaks in Fig. 10 are shown.


## ACKNOWLEDGMENTS

The support of the National Science Foundation Grant No. CHE-0132571 and the National Institutes of Health Grant No. GM59230-02A2 is gratefully acknowledged.


## APPENDIX: RELATING THE TRXR SIGNAL TO THE FORM-FACTOR

In order to simulate the vibrational dynamics semiclassically in terms of the MDCEOV dynamics code,[20] we transform the quantum expression [Eq. (7)] into a semiclassical expression [Eq. (8)].

Starting with Eq. (7) and neglecting the interference between $|e\rangle$ and $|e\beta\rangle$, we can write

$$\sum_{\nu,e}\mathrm{Tr}_{\mathrm{q}}[\langle e|\hat{\sigma}(\mathbf{r},t)|\nu\rangle\langle\nu|\hat{\sigma}(\mathbf{r}_3,t-t_3)|e\rangle\langle e|\hat{\rho}^{(2)}(t-t_3)|e\rangle]$$

$$=\sum_{\nu,e}\mathrm{Tr}_{\mathrm{q}}[e^{(i/\hbar)H_m^{(e)}(\mathrm{q})t_3}\langle e|\hat{\sigma}(\mathbf{r})|\nu\rangle e^{-(i/\hbar)H_m^{(\nu)}(\mathrm{q})t_3}$$

$$\times\langle\nu|\hat{\sigma}(\mathbf{r}_3)|e\rangle\langle e|\rho^{(2)}(t-t_3)|e\rangle],$$

$$=\sum_{\nu,e}\langle\langle\hat{\sigma}_{\nu e}(\mathbf{r})|\mathcal{G}_{\nu e}(t_3)\hat{\sigma}_{\nu e}(\mathbf{r}_3)|\rho_{ee}(t-t_3)\rangle\rangle, \qquad \text{(A1)}$$

where

$$\rho^{(2)}(t)\equiv\exp\left[-i\frac{i}{\hbar}\hat{H}_m(\mathrm{q})t\right]\hat{\rho}(t)\exp\left[i\frac{i}{\hbar}\hat{H}_m(\mathrm{q})t\right], \qquad \text{(A2)}$$

and the Liouville-space Green's function $\mathcal{G}_{\nu e}(t)$ is defined by its action on a nuclear-space operator $\hat{A}$ as follows:[26]

$$\mathcal{G}_{\nu e}(t_3)\hat{A} \equiv \theta(t_3)\exp\left[-\frac{i}{\hbar}H_m^{(\nu)}(\mathrm{q})t_3\right]\hat{A}\exp\left[\frac{i}{\hbar}H_m^{(e)}(\mathrm{q})t_3\right]. \tag{A3}$$

The coherence Green's function $\mathcal{G}_{\nu e}(t_3)$ can be split into a propagation with respect to the reference Hamiltonian $H_m^{(e)}$ and time-dependent phase whose evolution is again determined by $H_m^{(e)}$:[26]

$$\text{mathcal } G_{\nu e}(t_3)\hat{A} = \mathcal{G}_{ee}(t_3)\exp_+\left(-\frac{i}{\hbar}\int_0^{t_3}\Delta\hat{\Omega}_{\nu e}(\tau)d\tau\right)\hat{A}, \tag{A4}$$

where

$$\Delta\hat{\Omega}_{\nu e}(\tau) = \exp\left[\frac{i}{\hbar}H_m^{(e)}(\mathrm{q})\tau\right][\Omega_\nu(\mathrm{q}) - \Omega_e(\mathrm{q})] \times \exp\left[-\frac{i}{\hbar}H_m^{(e)}(\mathrm{q})\tau\right] \tag{A5}$$

represents the time-dependent transition energy between $|e\rangle$ and $|\nu\rangle$.

Substituting Eq. (A4) into (A1), we then have

$$\begin{aligned}
&\langle\langle \hat{\sigma}_{\nu e}(\mathbf{r})|\mathcal{G}_{\nu e}(t_3)\hat{\sigma}_{\nu e}(\mathbf{r}_3)|\rho_{ee}(t-t_3)\rangle\rangle \\
&= \left\langle \langle\hat{\sigma}_{\nu e}(\mathbf{r})|\mathcal{G}_{ee}(t_3) \times \exp_+\left[-\frac{i}{\hbar}\int_0^{t_3}\Delta\hat{\Omega}_{\nu e}(\tau)d\tau\right]\hat{\sigma}_{\nu e}(\mathbf{r}_3)|\rho_{ee}(t-t_3)\rangle\right\rangle \\
&= \left\langle \hat{\sigma}_{e\nu}(\mathbf{r},t)\exp_+\left[-\frac{i}{\hbar}\int_0^{t_3}\Delta\hat{\Omega}_{\nu e}(\tau)d\tau\right] \times \hat{\sigma}_{\nu e}(\mathbf{r}_3)\rho_{ee}(t-t_3)\right\rangle,
\end{aligned} \tag{A6}$$

where

$$\hat{\sigma}_{e\nu}(\mathbf{r},t) \equiv \exp\left[\frac{i}{\hbar}H_m^{(e)}t\right]\hat{\sigma}_{e\nu}(\mathbf{r})\exp\left[-\frac{i}{\hbar}H_m^{(e)}t\right]. \tag{A7}$$

In the classical approximation, quantum nuclear dynamics of $\hat{\sigma}_{e\nu}(\mathbf{r},t)$ and $\Delta\hat{\Omega}_{\nu e}(t)$ is replaced by a classical trajectory on the potential for $|e\rangle$. Since we treat $\Delta\hat{\Omega}_{\nu e}(t)$ as a classical quantity, we may further replace the time-ordered exponential by an ordinary exponential. The time-dependent charge density and phase can then be evaluated using classical trajectories obtained by Eq. (27). We then have

$$\hat{\Omega}_{\nu e}(t) = \Omega_{\nu e}[\mathrm{q}(t)] \tag{A8}$$

$$\hat{\sigma}_{e\nu}(\mathbf{r},t) = \sigma_{e\nu}[\mathbf{r},\mathrm{q}(t)] \tag{A9}$$

$$\begin{aligned}
&\left\langle \hat{\sigma}_{e\nu}(\mathbf{r},t)\exp_+\left[-\frac{i}{\hbar}\int_0^{t_3}\Delta\hat{\Omega}_{\nu e}(\tau)d\tau\right]\hat{\sigma}_{\nu e}(\mathbf{r}_3)\rho_{ee}(t-t_3)\right\rangle \\
&= \left\langle \sigma_{e\nu}(\mathbf{r},t)\exp\left[-\frac{i}{\hbar}\int_0^{t_3}\Delta\Omega_{\nu e}(\tau)d\tau\right]\sigma_{\nu e}(\mathbf{r}_3)\rho_{ee}(t-t_3)\right\rangle \\
&= \sigma_{e\nu}(\mathbf{r},t)\exp\left[-\frac{i}{\hbar}\int_0^{t_3}\Delta\Omega_{\nu e}(\tau)d\tau\right]\sigma_{\nu e}(\mathbf{r}_3,t-t_3).
\end{aligned} \tag{A10}$$

Performing the integration over $\mathbf{r}$ and $\mathbf{r}_3$ in Eq. (1) and using the definition of $\mu^{e\nu}(\Delta\mathbf{k})$ [Eq. (9)] finally gives Eq. (8).

When we consider a Gaussian probe pulse for $E_i(t)$ [Eq. (12)] with a short duration $\Delta T$ so that $\mathrm{q}(t)$ can be held constant during the time period $t_3$ in Eq. (A10), the TRXR signal Eq. (8) can be cast into

$$\begin{aligned}
W_{\mathrm{TRXR}} = &-\frac{2}{\omega_i^2}\Re\int_{-\infty}^{\infty}dt\int_0^{\infty}dt_3 E_i^*(t)E_i(t-t_3) \\
&\times\sum_\nu |\mu^{e\nu}(\Delta\mathbf{k};\mathrm{q}(t_0))|^2 \\
&\times\exp\{i[\Delta\omega - \Omega_\nu(\mathrm{q}(t_0)) + \Omega_e(\mathrm{q}(t_0))]t_3\}.
\end{aligned} \tag{A11}$$

Substituting Eq. (12) into Eq. (A11) and performing the time integrals, we obtain Eq. (13).


[1] M. Hentschel, R. Klenberger, Ch. Spielmann *et al.*, Nature (London) **414**, 519 (2001).
[2] M. Drescher, M. Hentshel, R. Kienberger, G. Tempea, C. Speilmann, G. A. Reider, P. B. Corkum, and F. Krausz, Science **291**, 1923 (2001).
[3] R. W. Schoenlein, S. Chattopadhyay, H. H. W. Chong, T. E. Glover, P. A. Heimann, C. V. Shank, A. A. Zholents, and M. S. Zolotorev, Science **287**, 2237 (2000).
[4] A. Rousse, C. Rischel, and J. C. Gauthier, Rev. Mod. Phys. **73**, 17 (2001).
[5] S. Tanaka and S. Mukamel, Phys. Rev. A **64**, 032503 (2001).
[6] S. Tanaka and S. Mukamel, J. Chem. Phys. **116**, 1877 (2002).
[7] S. Tanaka and S. Mukamel, Phys. Rev. Lett. **89**, 043001 (2002).
[8] P. M. Rentzepis and J. Helliwell, *Time-Resolved Electron and X-Ray Diffraction* (Oxford University Press, New York, 1995).
[9] A. H. Chin, R. W. Schoenlein, T. E. Glover, P. Balling, W. P. Leemans, and C. V. Shank, Phys. Rev. Lett. **83**, 336 (1999).
[10] C. R. Petruck, R. Jimenez, T. Guo, A. Cavalleri, C. W. Siders, F. Raski, J. A. Squier, B. C. Walker, K. R. Wilson, and C. P. J. Barty, Nature (London) **398**, 310 (1999).
[11] C. Bressler, M. Saes, M. Chergui, R. Abela, and P. Pattison, Nucl. Instrum. Methods Phys. Res. A **467**, 1444 (2000).
[12] L. X. Chen, W. J. H. Jäger, G. Jennings, D. J. Gosztola, A. Munkholm, and J. P. Hessler, Science **292**, 262 (2001).
[13] C. Bressler, M. Saes, M. Chegui, D. Arolimund, R. Abela, and P. Pattison, J. Chem. Phys. **116**, 2955 (2002).
[14] V. A. Lobastov, R. Srinivasan, B. M. Goodson, C.-Y. Ruan, J. S. Feenstra, and A. H. Zewail, J. Phys. Chem. A **105**, 11159 (2001).
[15] J. Cao and K. R. Wilson, J. Phys. Chem. **102**, 9523 (1998); M. Ben-Nun, J. Cao, and K. Wilson, J. Phys. Chem. A **101**, 8743 (1997).
[16] S. Tanaka, V. Chernyak, and S. Mukamel, Phys. Rev. A **63**, 063405 (2001).
[17] T. Kobayashi, A. Shirakawa H. Matsuzawa, and H. Nakanishi, Chem. Phys. Lett. **321**, 385 (2000).
[18] Corrected formulas for transition density matrices (unpublished).
[19] B. K. Agarwal, *X-ray Spectroscopy: An Introduction* (Springer-Verlag, Berlin, 1991).
[20] M. Tommasini, G. Zerbi, V. Chernyak, and S. Mukamel, J. Phys. Chem. **105**, 7057 (2001).
[21] V. Chernyak and S. Mukamel, J. Chem. Phys. **104**, 444 (1996).
[22] S. Tretiak V. Chernyak, and S. Mukamel, J. Am. Chem. Soc. **119**, 11408

(1997); Int. J. Quantum Chem. **70**, 711 (1998); S. Tretiak and S. Mukamel, Chem. Rev. **102**, 3171 (2002).
[23] See EPAPS Document No. E-JCPSA6-118-016305 for the transition density matrices for the lowest 50 excited states for Figs. 5 and 8. This document may be retrieved via the EPAPS homepage (http://www.aip.org/pubservs/epaps.html) or from ftp.aip.org in the directory /epaps/. See the EPAPS homepage for more information.
[24] J. Ridley and M. C. Zerner, Theor. Chim. Acta **32**, 111 (1973); M. C. Zerner, C. H. Loew, R. F. Kirchner, and U. T. Mueler-Westerhoff, J. Am. Chem. Soc. **102**, 589 (1980).
[25] V. J. Keast, A. J. Scott, R. Brydson, D. B. Williams, and J. Bruley, J. Microsc. **203**, 135 (2001).
[26] S. Mukamel, *Principles of Nonlinear Optical Spectroscopy* (Oxford University Press, New York, 1995).
[27] J. Zyss, I. Ledoux, S. Volkov, V. Chernyak, S. Mukamel, G. P. Bartholomew, and G. C. Bazan, J. Am. Chem. Soc. **122**, 11956 (2000).